

Improved lattice operators for non-relativistic fermions

Joaquín E. Drut

Theoretical Division, Los Alamos National Laboratory, Los Alamos, NM 87545-0001, USA

(Dated: November 4, 2021)

In this work I apply a recently proposed improvement procedure, originally conceived to reduce finite lattice spacing effects in transfer matrices for dilute Fermi systems, to tuning operators for the calculation of observables. I construct, in particular, highly improved representations for the energy and the contact, as a first step in an improvement program for finite-temperature calculations. I illustrate the effects of improvement on those quantities with a ground-state lattice calculation at unitarity.

PACS numbers: 03.75.Ss, 05.10.Ln, 12.38.Gc, 71.10.Fd

I. INTRODUCTION

One of the main sources of uncertainty in Monte Carlo (MC) calculations of lattice field theories stems from finite lattice spacing effects [1]. This is true in particular of non-relativistic systems at finite density, where the continuum limit is approached by taking the limit of diluteness, such that the interparticle distance $\sim k_F^{-1}$ (where k_F is the Fermi momentum) is much larger than the lattice spacing l . This is achieved in practice by first considering large volumes at fixed particle density, and then taking the zero-density limit. While this process is well defined, it is cumbersome to carry out, in part because calculations in large volumes require substantial amounts of CPU time. It is therefore useful to consider alternative approaches, based on effective field theory and renormalization group concepts [2, 3], which treat lattice-spacing effects by modifying the ultraviolet (UV) dynamics of the theory. In such formulations, lattice-spacing effects are eliminated at finite volume, even for densities that are not low by conventional standards.

In recent work, Endres et al. [4, 5] proposed a novel way to systematically reduce lattice-spacing effects in calculations of non-relativistic fermions. The method enables tuning of the lattice theory to high accuracy, such that the low end of the continuum energy spectrum is reproduced for the desired values of the two-body scattering parameters in the effective range expansion:

$$p \cot \delta(p) = -\frac{1}{a} + \frac{1}{2} r_{\text{eff}} p^2 + O(p^4), \quad (1)$$

where δ is the scattering phase shift, a is the scattering length, and r_{eff} is the effective range. The connection between the bare lattice theory (or rather its two-body spectrum) and these physical parameters is given by Lüscher's formula [7], which relates the phase shift to the energy $E = p^2/m$ of the two-body problem in a box of side L :

$$p \cot \delta(p) = \frac{1}{\pi L} \mathcal{S}(\eta) \quad (2)$$

where $\eta = \frac{pL}{2\pi}$ and

$$\mathcal{S}(\eta) \equiv \lim_{\Lambda \rightarrow \infty} \left(\sum_{\mathbf{n}} \frac{\Theta(\Lambda^2 - \mathbf{n}^2)}{\mathbf{n}^2 - \eta^2} - 4\pi\Lambda \right), \quad (3)$$

where the sum is over all 3D integer vectors (the evaluation of $\mathcal{S}(\eta)$ is discussed in Appendix A), and $\Theta(x)$ is the Heaviside function. Throughout this work, we shall take units such that $\hbar = k_B = m = 1$, where m is the mass of the fermions.

The two-body matching condition described above completely specifies the physics of dilute systems, such as those currently realized with ultracold atomic gases (see e.g. Ref. [6] for a review of the experimental situation). In this work we shall restrict ourselves to such systems, neglecting the additional complications that arise for instance at higher densities or for nuclear systems, where three- and higher-body forces play an important role.

We shall briefly review the work of Ref. [4] below, but it is useful to mention the main steps underlying the method at this point. First, one writes down the transfer matrix \mathcal{T} , representing the two-body interaction via a generalized Hubbard-Stratonovich (HS) transformation [8, 9]. The latter contains $N_{\mathcal{O}}$ arbitrary coefficients C_n . The matrix elements of \mathcal{T} are then computed in the subspace of two particles at vanishing total momentum. The resulting matrix is then diagonalized in the s -wave subspace (or rather its lattice equivalent), and the HS coefficients C_n are tuned using an iterative algorithm such that the eigenvalues of the proposed \mathcal{T} match $\exp(-\tau E)$, where τ is the temporal discretization parameter and E are the energies dictated by Lüscher's formula, for the desired box size L and choice of scattering parameters.

In the case of the unitary limit, where by definition

$$p \cot \delta(p) \equiv 0, \quad (4)$$

the above procedure yields considerable improvement in the approach to the continuum. Indeed, with a single coefficient C_0 (the simplest case, discussed in Sec. II) one may tune the scattering length a , but the effective range r_{eff} remains finite due to lattice-spacing artifacts. Naturally, by introducing more parameters one may tune the

effective-range expansion in Eq. (1) to higher accuracy, thus systematically eliminating the need for extrapolations to the dilute limit and leaving only finite-volume effects unaccounted for.

It is the main objective of this work to extend the approach of Ref. [4] to designing not only improved transfer matrices but also improved operators for the calculation of observables. This is an important step toward reducing lattice-spacing effects in finite-temperature calculations. While these effects were studied at unitarity in Ref. [10] for the Hubbard model using dynamical mean-field theory, careful systematic studies in full-fledged MC calculations have only recently started to appear [4, 5, 11, 12] and are still restricted to the ground state. Interestingly, recent studies based on functional renormalization group techniques [13] have also started to tackle the problem of extrapolating to infinite volume and particle number in the unitary limit.

In Sec. II we analyze a basic example, as a primer to reviewing the more sophisticated formalism of Ref. [4], which we explain briefly in Sec. III. In Sec. IV we present the main developments of this work, with the corresponding illustrative results and conclusions appearing in Sec. V. Finally, some of the less trivial numerical issues are explained in the Appendix.

II. A SIMPLE EXAMPLE

Before proceeding to a more detailed discussion, let us analyze a simple case, to fix notation as well as ideas. Consider the following lattice Hamiltonian:

$$\hat{H} \equiv \sum_{\mathbf{k}, s=\uparrow, \downarrow} \frac{k^2}{2m} \hat{a}_{s, \mathbf{k}}^\dagger \hat{a}_{s, \mathbf{k}} - g \sum_{\mathbf{i}} \hat{n}_{\uparrow, \mathbf{i}} \hat{n}_{\downarrow, \mathbf{i}}, \quad (5)$$

where s denotes the spin projection, g is the bare lattice coupling constant, and $\hat{n}_{s, \mathbf{i}} \equiv \hat{a}_{s, \mathbf{i}}^\dagger \hat{a}_{s, \mathbf{i}}$ denotes the number density operator at lattice position \mathbf{i} for spin projection s . The value of g is tuned to the desired two-body scattering properties by solving the two-body problem on the lattice and finding the scattering amplitude, which in this case can be done analytically.

The transfer matrix is then expressed approximately in powers of the imaginary time step τ using a Suzuki-Trotter decomposition, for instance as follows:

$$\mathcal{T} \equiv e^{-\tau \hat{H}} \simeq e^{-\frac{\tau \hat{T}}{2}} e^{-\tau \hat{V}} e^{-\frac{\tau \hat{T}}{2}} + O(\tau^2), \quad (6)$$

where

$$\hat{T} \equiv \sum_{\mathbf{k}} \hat{T}_\uparrow + \hat{T}_\downarrow, \quad \hat{T}_s \equiv \sum_{\mathbf{k}} \frac{k^2}{2m} \hat{a}_{s, \mathbf{k}}^\dagger \hat{a}_{s, \mathbf{k}}, \quad (7)$$

$$\text{and } \hat{V} \equiv -g \sum_{\mathbf{i}} \hat{n}_{\uparrow, \mathbf{i}} \hat{n}_{\downarrow, \mathbf{i}}. \quad (8)$$

The kinetic energy factor in Eq. (6) is easy to treat, as it is an exponential of a one-body operator which is diagonal in momentum space. Notice that we have chosen to

define the dispersion relation $E = k^2/2m$ in momentum space, as opposed to defining it via a discrete representation of the Laplacian operator in coordinate space (which is common in Hubbard-model type formulations).

On the other hand, the potential energy factor represents a challenge, as it is the exponential of a non-trivial two-body operator (as the original Hamiltonian). It is at this point that the HS transformation plays a central role, allowing us to exchange the complexity of the two-body operator for a path integral involving only one-body operators. Specifically, we write

$$\begin{aligned} \exp(-\tau \hat{V}) \prod_{\mathbf{i}} \exp(\tau g \hat{n}_{\uparrow, \mathbf{i}} \hat{n}_{\downarrow, \mathbf{i}}) \\ = \int \mathcal{D}\sigma \prod_{\mathbf{i}} \left(1 + \sqrt{A} \hat{n}_{\uparrow, \mathbf{i}} \sin \sigma_{\mathbf{i}}\right) \left(1 + \sqrt{A} \hat{n}_{\downarrow, \mathbf{i}} \sin \sigma_{\mathbf{i}}\right) \end{aligned} \quad (9)$$

where $A = 2(e^{\tau g} - 1)$, $\mathcal{D}\sigma = \prod_{\mathbf{i}} d\sigma_{\mathbf{i}}/(2\pi)$, and $\sigma_{\mathbf{i}}$ is an external auxiliary field. In this way, one decouples the transfer matrix for each spin, such that we may write

$$\mathcal{T} = \int \mathcal{D}\sigma \mathcal{T}_\uparrow[\sigma] \mathcal{T}_\downarrow[\sigma] \quad (10)$$

where, up to order τ^2 ,

$$\mathcal{T}_s[\sigma] = e^{-\frac{\tau \hat{T}_s}{2}} \prod_{\mathbf{i}} \left(1 + \sqrt{A} \hat{n}_{s, \mathbf{i}} \sin \sigma_{\mathbf{i}}\right) e^{-\frac{\tau \hat{T}_s}{2}}, \quad (11)$$

which in the one-particle subspace reduces to

$$\mathcal{T}_s[\sigma] = e^{-\frac{\tau \hat{T}_s}{2}} \left(1 + \sqrt{A} \sum_{\mathbf{i}} \hat{n}_{s, \mathbf{i}} \sin \sigma_{\mathbf{i}}\right) e^{-\frac{\tau \hat{T}_s}{2}}. \quad (12)$$

Notice that in Eq. (9) we have used a version of the HS transform due to Lee [19], in which the auxiliary field is continuous and compact (the integral is restricted to the interval $[-\pi, \pi]$), as opposed to more conventional versions that are discrete, or continuous but unbounded. Apart from the path integral, at this point applying the transfer matrix becomes a problem of applying a product of one-body operators, which one can easily deal with.

All of the above steps are standard in the literature of many-body MC calculations, except perhaps for the use of a “perfect” dispersion relation defined in momentum space, which has become more common only in recent years [11, 15]. This feature can be regarded as a basic kind of improvement, as it reduces lattice-spacing effects relative to Hubbard-model approaches, where $dE/dk \rightarrow 0$ at high momenta.

This example captures the main features of most modern many-fermion MC calculations. Nevertheless, the simplicity of this approach is in some ways excessive, largely because we only have one coupling constant at our disposal. Indeed, should we desire to fix more than one coefficient in the effective-range expansion, we would need a richer bare interaction, and a correspondingly more sophisticated HS transformation. In this simple case, to reach for instance the unitary limit, we can tune

the scattering length, but we also need to consider very dilute systems to avoid the effects of finite range induced by the UV lattice cutoff π/l , as in that case one has $r_{\text{eff}} \simeq 0.40l$. Moreover, taking for example 80 particles in a 10^3 lattice volume, which shall be our illustrative example below, one finds $k_F r_{\text{eff}} \simeq 0.54$, which is not nearly as small as one would like.

As mentioned before, one can resort to alternative approaches that modify the Hamiltonian by including higher-order terms in a low-momentum expansion, tuning the corresponding couplings to eliminate UV effects. The latter strategy is essentially what Ref. [4] advocates, following the spirit of the Lattice QCD program initiated by Symanzik many years ago [3] to design improved effective actions that approach the continuum limit (see e.g. Ref. [14]). Since it will be useful for the rest of this work, we shall briefly review the method of Ref. [4] in the next section.

III. IMPROVED TRANSFER MATRICES

The work of Ref. [4] tackles the problem of reducing UV lattice effects by defining an improved transfer matrix, using a generalized HS transformation and a low-momentum expansion. This is accomplished by allowing the constant A to have a non-trivial momentum dependence. For simplicity, it is useful to take $A(\mathbf{p})$ to be diagonal in momentum space. Following Ref. [4], we expand $A(\mathbf{p})$ using a set of operators as

$$A(\mathbf{p}) = \sum_{n=0}^{N_{\mathcal{O}}-1} C_n \mathcal{O}_n(\mathbf{p}), \quad (13)$$

where one may choose to define, for convenience,

$$\mathcal{O}_n(\mathbf{p}) = \left(1 - e^{-\mathbf{p}^2}\right)^n, \quad (14)$$

as done in Ref. [4] (up to an n -dependent constant in front), or, as we shall use in the rest of this work,

$$\mathcal{O}_n(\mathbf{p}) = [2 \sin(p/2)]^{2n}. \quad (15)$$

Notice that this last expression contains only even powers of $p = \sqrt{\mathbf{p}^2}$, and is therefore an analytic function of the momentum \mathbf{p} . Both of the above choices for $\mathcal{O}_n(\mathbf{p})$ behave as $\sim p^{2n}$ at low momenta. For the purposes of Monte Carlo calculations, the operator $A(\mathbf{p})$ can be computed once and for all at the beginning of the calculation, and is applied at each time slice using Fourier transforms.

In order to determine the coefficients C_n , we find the explicit form of \mathcal{T} for two particles, which upon integrating the auxiliary field is given in momentum space by

$$\begin{aligned} \mathcal{T}_2(\mathbf{p}_\uparrow \mathbf{p}_\downarrow; \mathbf{q}_\uparrow \mathbf{q}_\downarrow) e^{-\frac{\tau T(\mathbf{p})}{2}} & \left[\delta_{\mathbf{p}_\uparrow \mathbf{q}_\uparrow} \delta_{\mathbf{p}_\downarrow \mathbf{q}_\downarrow} \right. \\ & \left. + \frac{\sqrt{A(\mathbf{p}_\uparrow)} \sqrt{A(\mathbf{p}_\downarrow)}}{2V} \delta_{\mathbf{p}_\uparrow + \mathbf{p}_\downarrow, \mathbf{q}_\uparrow + \mathbf{q}_\downarrow} \right] e^{-\frac{\tau T(\mathbf{q})}{2}}, \quad (16) \end{aligned}$$

where V is the lattice volume and $T(k) = (\mathbf{k}_\uparrow^2 + \mathbf{k}_\downarrow^2)/2m$. One cannot fail to notice that the above transfer matrix is not Galilean invariant. We elaborate on this issue in the appendices. In this work we shall take $\Lambda = \pi(1 - 10^{-5})$, following the steps of Ref. [4]. The operators in Eqs. (14) and (15) are defined to be constant above $p^2 = \Lambda^2$, and the kinetic energy factor $\exp(-\tau T/2)$ is defined to vanish above that boundary, such that there is no propagation for $p^2 \geq \Lambda^2$.

Evaluating \mathcal{T}_2 in the center-of-mass frame, we have

$$\mathcal{T}_2(\mathbf{p}_r; \mathbf{q}_r) = e^{-\frac{\tau p_r^2}{2m}} \left[\delta_{\mathbf{p}_r \mathbf{q}_r} + \frac{A(\mathbf{p}_r)}{2V} \right] e^{-\frac{\tau q_r^2}{2m}}, \quad (17)$$

where \mathbf{p}_r and \mathbf{q}_r are incoming and outgoing relative momenta. By diagonalizing this expression, we may identify the eigenvalues of \mathcal{T}_2 with $e^{-\tau E}$, where E are the two-particle eigenvalues of the Hamiltonian we are implicitly defining.

One may then tune the C_n such that this energy spectrum matches the one required by Lüscher's formula for the lowest $N_{\mathcal{O}}$ eigenvalues, given the desired values of the scattering parameters in Eq. (1), and using $E = p^2/m = \eta^2(2\pi)^2/(mL^2)$. Specifically, if we are interested in describing the unitary limit, the eigenvalues are determined by the zeros of the function $S(\eta)$ in Eq. (3). The actual fitting of the C_n can be performed iteratively, as described in detail in Ref. [4]. Notice, in particular, that our expression for \mathcal{T}_2 ceases to be Hermitian when we promote A to be an operator. Therefore, one needs to use $\mathcal{T}_2^\dagger \mathcal{T}_2$ rather than \mathcal{T}_2 to diagonalize and fit the eigenvalues, as well as for the actual Monte Carlo calculations.

The results of our fits for C_n are shown in Table I. The quality of the improvement can be assessed by plotting $p \cot \delta(p)$ as a function of η^2 , which is shown in Fig. 1 for $N_x = 20$, $\tau = 0.05$, and $N_{\mathcal{O}} = 1 - 5$. As can be appreciated in the figure, the same effect is achieved as in Ref. [4]: as the order of the expansion is increased, the transfer matrix is accurately tuned to unitarity up to progressively higher momenta.

IV. IMPROVED OBSERVABLES

The above procedure represents a significant step forward in mitigating lattice-spacing effects in MC calcula-

TABLE I. Results of fitting the coefficients C_n (see Sec. III) to the low-energy spectrum of the two-body problem at resonance, in a box of side $N_x = 16$, for an imaginary time step $\tau = 0.05$, in lattice units.

$N_{\mathcal{O}}$	C_0	C_1	C_2	C_3	C_4
1	0.68419	–	–	–	–
2	0.53153	0.07896	–	–	–
3	0.49278	0.04366	0.01807	–	–
4	0.47217	0.03711	0.00784	0.00467	–
5	0.45853	0.03331	0.00718	0.00132	0.00129

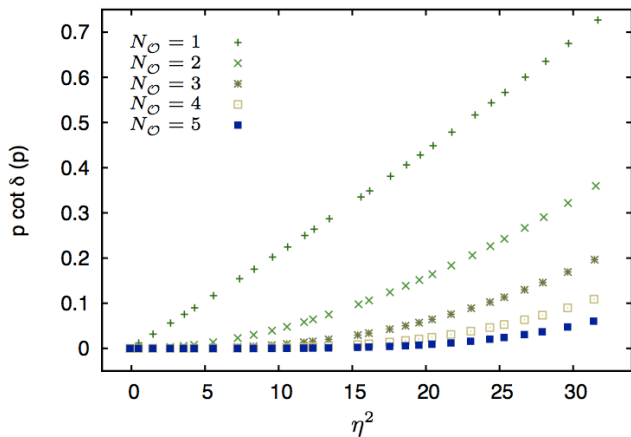


FIG. 1. (Color online) Plot of $p \cot \delta(p)$, in lattice units, as a function of $\eta^2 = E_2/p_0^2$ (where $p_0 \equiv 2\pi/L$), for $N_x = 20$, $\tau = 0.05$, and levels of improvement $N_{\mathcal{O}} = 1-5$, for a Galilean non-invariant definition of the transfer matrix (for $N_{\mathcal{O}} > 2$).

tions, especially considering that it requires only a small coding investment for its implementation in extant MC codes, and it results in minimal computational overhead.

A somewhat unsettling issue remains, however, particularly in connection with improving finite temperature lattice calculations, such as those of Refs. [15–17]. Indeed, in those calculations, as well as in similar ground-state approaches, the transfer matrix is not the only object carrying lattice-spacing effects: the operators used to compute expectation values also suffer from the same problems. The situation may appear problematic at first sight, as the improvement strategy defined above does not directly define improved operators that we could use to compute observables at finite temperature.

On the other hand, in conventional formulations, knowledge of the explicit τ dependence of the transfer matrix (as in the simple example described in Sec. II) allows us to take a derivative that brings the Hamiltonian down from the exponent (c.f. Eqs. (10) and (11)), which results in a practical expression for the calculation of the energy [?].

To fix ideas, let us consider the grand canonical ensemble (see also Ref. [15, 18]), where the partition function satisfies, by definition,

$$\mathcal{Z} = e^{-\beta\Omega}. \quad (18)$$

Averages of observables can be extracted from knowledge of \mathcal{Z} through derivatives, and in particular the energy is obtained by means of

$$-\frac{\partial \log \mathcal{Z}}{\partial \beta} = E - \mu N. \quad (19)$$

When using the formalism derived in Sec. II, we have (assuming the system is unpolarized)

$$\mathcal{Z} = \text{Tr} [\mathcal{T}^{N_\tau}] = \int \mathcal{D}\sigma \det [1 + \mathcal{U}[\sigma]]^2, \quad (20)$$

where

$$\mathcal{T}^{N_\tau} = \int \mathcal{D}\sigma \prod_t \mathcal{T}_\uparrow[\sigma_t] \mathcal{T}_\downarrow[\sigma_t], \quad (21)$$

$$\beta = \tau N_\tau, \quad (22)$$

and where now σ is to be regarded as a space-time varying field, and σ_t is σ restricted to the t -th imaginary-time slice. The determinant is to be taken in the subspace of one-particle states, and

$$\mathcal{U}[\sigma] \equiv \prod_t \mathcal{T}_\uparrow[\sigma_t]. \quad (23)$$

As the derivative in Eq. (19) becomes now a derivative with respect to τ , it is clear that all we require is knowing how to differentiate \mathcal{T}_s with respect to τ , because

$$-\frac{\partial \log \mathcal{Z}}{\partial \tau} = \frac{1}{\mathcal{Z}} \int \mathcal{D}\sigma \det [1 + \mathcal{U}]^2 \text{Tr} \left[\frac{\partial \mathcal{U} / \partial \tau}{1 + \mathcal{U}} \right], \quad (24)$$

where

$$\frac{\partial \mathcal{U}}{\partial \tau} = \sum_{t_0} \prod_{t > t_0} \mathcal{T}_\uparrow[\sigma_t] \frac{\partial \mathcal{T}_\uparrow[\sigma_{t_0}]}{\partial \tau} \prod_{t < t_0} \mathcal{T}_\uparrow[\sigma_t]. \quad (25)$$

We shall take the point of view that differentiation of partition functions with respect to parameters in the Hamiltonian is the proper way to obtain expectation values of operators. We shall then generalize the improvement procedure of Ref. [4] to design highly improved operators (in particular for the energy and the contact) and accomplish this by taking formal derivatives of the transfer matrix and writing them in an operator expansion, fitting the expansion coefficients to reproduce the low end of the exact two-particle spectra. By "highly improved" we mean improvements that go well beyond tuning the first two coefficients in the effective-range expansion.

While in the above example we have focused on the calculation of the energy, which we resume in the next section, similar derivations apply for the calculation of the contact, as we shall see in Sec. IV B.

A. Energy

In the simple case presented in Sec. II, the calculation of the first τ derivative results in the following expression:

$$-\frac{\partial \mathcal{T}_s[\sigma]}{\partial \tau} = e^{-\frac{\tau \hat{T}_s}{2}} (\hat{K} + \hat{U}_\tau) e^{-\frac{\tau \hat{T}_s}{2}} \quad (26)$$

where \hat{K} is the following anticommutator

$$\hat{K} \equiv \left\{ \frac{\hat{T}_s}{2}, (1 + \sqrt{A} \sum_i \hat{n}_{s,i} \sin \sigma_i) \right\}, \quad (27)$$

and

$$\hat{U}_\tau \equiv -\frac{\partial \sqrt{A}}{\partial \tau} \sum_i \hat{n}_{s,i} \sin \sigma_i. \quad (28)$$

The derivative of \sqrt{A} with respect to τ appearing in Eq. (28) is known analytically in this case. When using improved transfer matrices, however, that derivative is somewhat harder to compute, as we only know the coefficients C_n in Eq. (13) as a result of a numerical fit, which complicates the calculation of $\partial C_n/\partial\tau$.

Here we extend the procedure of Endres et al. to fitting the coefficients in the expansion of the derivative of $A(\mathbf{p})$. There are at least two advantages in following this route over computing the derivatives via finite differences. In the first place, the fitting procedure can provide a much more accurate determination of the expansion coefficients of the derivative, with less effort. (That being said, finite differences do provide a useful starting point for the fitting routine.) Secondly, this route allows one to use different operators for different observables, regardless of what is used for $A(\mathbf{p})$ itself. This feature can potentially be very convenient: different observables are in general sensitive to different regions of momentum space, such that there is no a priori reason why a given set of operators \mathcal{O}_n should be universally useful.

The main idea behind the method remains the same as in Ref. [4]. Lüscher's formula provides us with the exact two-particle spectrum, such that the eigenvalues of the exact two-particle transfer matrix and its τ derivative(s) are known:

$$-\frac{\partial \mathcal{T}_2^{\text{exact}}}{\partial \tau} = E_2 \exp(-\tau E_2) \quad (29)$$

where E_2 are the exact two-particle energies in a continuous box [?].

In order to match this spectrum, we take the derivative of Eq. (17) with respect to τ , evaluated between eigenstates $|E\rangle$ of the proposed transfer matrix \mathcal{T}_2 . We thus obtain, using the Feynman-Hellmann theorem,

$$-\frac{\partial \langle E | \mathcal{T}_2 | E \rangle}{\partial \tau} = \langle E | e^{-\frac{\tau p_r^2}{2m}} [K_2 + U_2] e^{-\frac{\tau q_r^2}{2m}} | E \rangle, \quad (30)$$

where

$$K_2 \equiv \left[\frac{p_r^2}{2m} + \frac{q_r^2}{2m} \right] \left[\delta_{\mathbf{p}, \mathbf{q}_r} + \frac{A(\mathbf{p}_r)}{2V} \right] \quad (31)$$

and

$$U_2 \equiv -\frac{1}{2V} \frac{\partial A(\mathbf{p}_r)}{\partial \tau} = \frac{1}{2V} \sum_{n=0}^{N_{\text{max}}-1} D_n \mathcal{O}_n(\mathbf{p}_r). \quad (32)$$

The rest of the recipe consists in taking the right-hand side of Eq. (30) and fitting the coefficients D_n such that the first N_{max} eigenvalues of the exact expression Eq. (29) (which correspond to the lowest eigenvalues prescribed by Lüscher's formula) are reproduced. We may assume at this point that the coefficients C_n are known, such that the eigenvectors $|E\rangle$ are fixed when we set out to find the D_n . In that case, the D_n are determined by a linear system of equations of order $N_{\text{max}} \times N_{\text{max}}$:

$$\sum_{n=0}^{N_{\text{max}}-1} M_{En} D_n = Y_E \quad (33)$$

TABLE II. Results of fitting the coefficients D_n (see Sec. IV) to the low-energy spectrum of the two-body problem at resonance, in a box of side $N_x = 16$, for an imaginary time step $\tau = 0.05$, in lattice units.

$N_{\mathcal{O}}$	D_0	D_1	D_2	D_3	D_4
1	-14.76869	–	–	–	–
2	-11.54894	-1.74519	–	–	–
3	-10.74506	-0.96946	-0.40164	–	–
4	-10.31974	-0.82605	-0.17494	-0.10404	–
5	-10.03874	-0.74266	-0.16064	0.02948	-0.02878

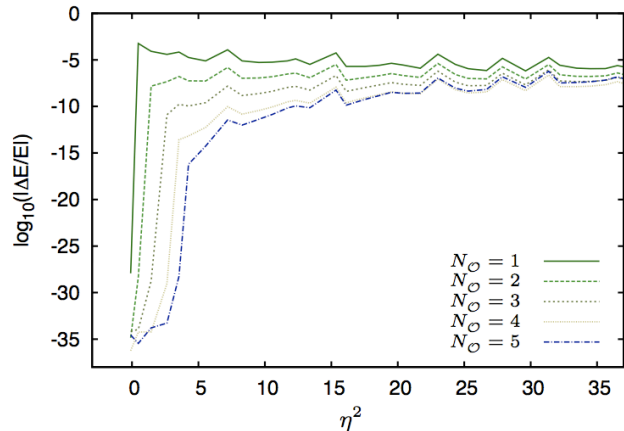


FIG. 2. (Color online) Logarithmic plot of the difference between the exact spectrum of the two-body problem Eq. (29) at unitarity, and the approximate spectrum obtained with various levels of improvement $N_{\mathcal{O}} = 1-5$, relative to the exact spectrum (see text for details), as a function of $\eta^2 = E_2/p_0^2$, where $p_0 \equiv 2\pi/L$. The original data are discrete; the lines are intended as a guide to the eyes. These results correspond to a lattice of side $N_x = 20$ and temporal spacing $\tau = 0.05$.

where

$$M_{En} = \frac{1}{2V} \langle E | \mathcal{O}_n | E \rangle \quad (34)$$

and

$$Y_E = E \exp(-\tau E) - \langle E | e^{-\frac{\tau p_r^2}{2m}} K_2 e^{-\frac{\tau q_r^2}{2m}} | E \rangle \quad (35)$$

Once the coefficients D_n have been determined, one can use Eq. (28) in a lattice calculation simply by replacing $A \rightarrow A(\mathbf{p})$, and taking $\partial C_n/\partial\tau = D_n$. The results of the fits for C_n , D_n are shown in Tables I and II.

As a first illustration of the level of improvement that can be achieved for the energy, Fig. 2 shows the difference between the approximate spectrum with various levels of improvement E_{approx} and the exact spectrum E_{exact} , as a function of η^2 , through the quantity $\text{Log}(|\Delta E|)$, where $\Delta E = (E_{\text{approx}} - E_{\text{exact}})/E_{\text{exact}}$. As expected, with each new parameter a new eigenvalue is reproduced, with the concomitant reduction in the error.

Surprisingly, the approximations perform well considerably beyond the lowest eigenvalues that are fit. Indeed, with each new level of improvement we see, apart from a dramatic reduction in the error for the target eigenvalues, an extra reduction in the error that is evident even beyond $\eta^2 \simeq 30$.

B. Contact

One of the many ways to define the contact C (see Refs. [20, 21]) is through the derivative of the energy with respect to the inverse scattering length:

$$\frac{\partial E}{\partial a^{-1}} = -\frac{\hbar^2}{4\pi m} C. \quad (36)$$

Since E may be obtained directly from the logarithm of the partition function, we are again in a situation where we require a derivative of the transfer matrix with respect to a parameter, in this case a^{-1} . The generalization of the above definition to finite temperature in the grand canonical ensemble is

$$\left(\frac{\partial \Omega}{\partial a^{-1}} \right)_{T,\mu} = -\frac{1}{\beta} \left(\frac{\partial \log \mathcal{Z}}{\partial a^{-1}} \right)_{T,\mu} = -\frac{\hbar^2}{4\pi m} C, \quad (37)$$

where Ω is the grand thermodynamic potential, T is the temperature and μ is the chemical potential.

In many-body lattice calculations, using these definitions involves the following expression:

$$\frac{\partial \mathcal{T}_s[\sigma]}{\partial a^{-1}} = e^{-\frac{\tau \hat{r}_s}{2}} \hat{U}_{a^{-1}} e^{-\frac{\tau \hat{r}_s}{2}} \quad (38)$$

where

$$\hat{U}_{a^{-1}} \equiv \frac{\partial \sqrt{A}}{\partial a^{-1}} \sum_i \hat{n}_{s,i} \sin \sigma_i. \quad (39)$$

The first step towards using these expressions in combination with the improvement procedure is to take a formal derivative of \mathcal{T} with respect to a^{-1} in the two-particle space, which we can treat exactly:

$$\frac{\partial \mathcal{T}_2^{\text{exact}}}{\partial a^{-1}} = -\tau \frac{\partial E_2}{\partial a^{-1}} \exp(-\tau E_2). \quad (40)$$

In order to compute the change in the exact two-particle energy E_2 due to a small change in the inverse scattering length, we use the fact that the energies are implicitly defined as solutions of Eq. (2), which implies

$$\frac{\partial E_2}{\partial a^{-1}} = -\frac{4\pi^3}{L} \left(\frac{d\mathcal{S}}{d\eta^2} \right)^{-1} \quad (41)$$

where $\eta^2 = E_2 L^2 / (2\pi)^2$, and the derivative on the right-hand side is to be evaluated at the corresponding solution of Eq. (2). Table IV in the Appendix shows the first 30 roots of $S(\eta)$ and the corresponding values of $d\mathcal{S}/d\eta^2$.

TABLE III. Results of fitting the coefficients F_n (see Sec. IV) to the low-energy spectrum of the two-body problem at resonance, in a box of side $N_x = 16$, for an imaginary time step $\tau = 0.05$, in lattice units.

$N_{\mathcal{O}}$	F_0	F_1	F_2	F_3	F_4
1	0.36773	–	–	–	–
2	0.14532	0.07568	–	–	–
3	0.11370	0.02220	0.01957	–	–
4	0.09659	0.01695	0.00415	0.00538	–
5	0.08205	0.01278	0.00406	-0.00023	0.00180

In the derivation of Eq. (41), we have assumed that all the effective-range parameters other than the scattering length are kept constant.

Having the exact target spectrum, we proceed by finding the corresponding expression in terms of the HS function $A(\mathbf{p})$, which we obtain using Eq. (17) and the Feynman-Hellmann theorem:

$$\frac{\partial \langle E | \mathcal{T}_2 | E \rangle}{\partial a^{-1}} = \langle E | e^{-\frac{\tau \hat{p}_r^2}{2m}} \frac{1}{2V} \frac{\partial A(\mathbf{p}_r)}{\partial a^{-1}} e^{-\frac{\tau \hat{p}_r^2}{2m}} | E \rangle, \quad (42)$$

where, as before, we expand in terms of our chosen set of operators,

$$\frac{\partial A(\mathbf{p}_r)}{\partial a^{-1}} = \sum_{n=0}^{N_{\text{max}}} F_n \mathcal{O}_n(\mathbf{p}_r), \quad (43)$$

and we determine the coefficients F_n by fitting the diagonal matrix elements in the right-hand side of Eq. (42) to the exact spectrum of Eqs. (40) and (41). As with the energy, the fitting procedure can be reduced to solving a set of linear equations of order $N_{\text{max}} \times N_{\text{max}}$. Illustrative results of such a fit are shown in Table III.

As with the energy, a first glimpse at the level of improvement that can be obtained at this point. This is shown in Fig. 3, where we display the difference ΔC between the spectrum with various levels of improvement and the exact spectrum, divided by the latter. As in Fig. 2, each new parameter allows one to fit a new eigenvalue to high accuracy, matching the desired physics beyond the lowest momentum.

Unlike in Fig. 2, the improvement for eigenvalues beyond those explicitly fit is limited, breaking down after the eighth or ninth eigenvalue. From that point on toward higher energies, little improvement, if any, is observed as the order of the expansion is increased. This behavior is only unexpected in the light of Fig. 2, where the situation is (surprisingly) much more favorable. Possibly, part of the reason for this behavior is that the target spectra for the energy and the transfer matrix are monotonic (either increasing or decreasing) at low energies, whereas the one for the contact is closer to a random sequence (see Table IV in the Appendix).

On the other hand, as mentioned before, there is no reason to believe that a given choice of operators will be equally useful for all observables. It is therefore natural

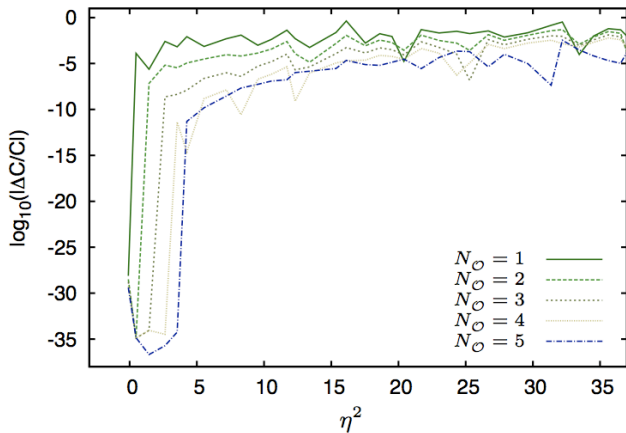


FIG. 3. (Color online) Logarithmic plot of the difference between the exact two-body spectrum Eq. (40) at unitarity, and the spectrum obtained with various levels of improvement $N_{\mathcal{O}} = 1 - 5$, relative to the exact spectrum (see text for details), as a function of $\eta^2 = E_2/p_0^2$, where $p_0 \equiv 2\pi/L$. The original data are discrete; the lines are intended as a guide to the eyes. These results correspond to a lattice of side $N_x = 16$ and temporal spacing $\tau = 0.05$.

to suspect that a different set of operators could yield a better expansion for the contact. This possibility remains to be studied.

C. Extrapolation to the ground state

Taking a Slater-determinant state $|\psi_0\rangle$ as a starting point, it is easy to see that the probability sum in ground-state calculations, for a temporal extent β can be written as

$$\mathcal{Z}_0(\beta) = \sum_k A_k e^{-\beta E_k}, \quad (44)$$

where E_k are the exact energy eigenvalues and

$$A_k \equiv |\langle \psi_0 | E_k \rangle|^2. \quad (45)$$

Taking a derivative of $\log \mathcal{Z}_0(\beta)$ with respect to τ it is easy to see that in the large- β limit one can write

$$E(\beta) \equiv -\frac{\partial \log \mathcal{Z}_0(\beta)}{\partial \beta} \rightarrow E_0 + b_E e^{-\beta \delta}, \quad (46)$$

where E_0 is the ground-state energy, $\delta = E_1 - E_0$, and

$$b_E = \frac{A_1}{A_0} (E_1 - E_0). \quad (47)$$

Similarly, taking a derivative with respect to a^{-1} one can see that the first few leading contributions to the asymptotic behavior at large β are given by

$$C(\beta) \equiv \frac{4\pi m}{\hbar^2 \beta} \frac{\partial \log \mathcal{Z}_0(\beta)}{\partial a^{-1}} \rightarrow C_0 + b_{C1} \beta^{-1} + b_{C2} e^{-\beta \delta} \quad (48)$$

where C_0 is the ground-state contact,

$$b_{C1} = \frac{4\pi m}{\hbar^2} \frac{\partial \log A_0}{\partial a^{-1}}, \quad (49)$$

$$b_{C2} = -\frac{4\pi m}{\hbar^2} \frac{A_1}{A_0} \left(\frac{\partial E_1}{\partial a^{-1}} - \frac{\partial E_0}{\partial a^{-1}} \right). \quad (50)$$

We shall use these expressions to motivate the extrapolations to the $\beta \rightarrow \infty$ limit below.

V. ILLUSTRATIVE RESULTS AND CONCLUSIONS

To illustrate the effect of improved operators in real-time lattice calculations, this section presents the results of ground-state MC calculations of the energy (Fig. 4) and the contact (Fig. 5), for an unpolarized system at unitarity.

Results are shown for 80 particles (40 per spin) in a volume of 10^3 lattice points, for various levels of improvement $N_{\mathcal{O}} = 1 - 4$. In each case, calculations were performed for time directions of extent $\beta \epsilon_F = 2.0 - 8.0$ (corresponding to N_τ roughly between 40 and 200), subsequently extrapolating to the $\beta \rightarrow \infty$ limit. We have taken $\tau = 0.05$ in lattice units, and a Slater determinant of plane waves as the starting guess for the ground-state wavefunction. For each value of β , we obtained approximately 400 samples of the auxiliary field σ . The statistics is enhanced by a factor of 20 - 100 by the fact that the operators we have defined utilize every other time slice. Some obvious fluctuations remain, as evident from some degree of jaggedness in the data. This can be resolved by increasing the statistics, but it does not affect our main conclusions.

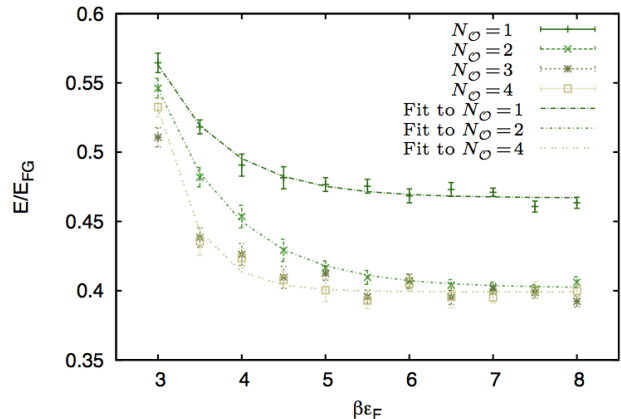


FIG. 4. (Color online) Energy, in units of $E_{FG} = \frac{3}{5} N \epsilon_F$, as a function of the extent of the time direction $\beta \epsilon_F = \tau N_\tau \epsilon_F$, for 80 particles and levels of improvement $N_{\mathcal{O}} = 1 - 4$.

Once the improvements are turned on, i.e. for $N_{\mathcal{O}} = 2 - 4$, we see that the change from $k_{F \text{ eff}} \simeq 0.54$ to $k_{F \text{ eff}} = 0$ results in a considerable reduction in the

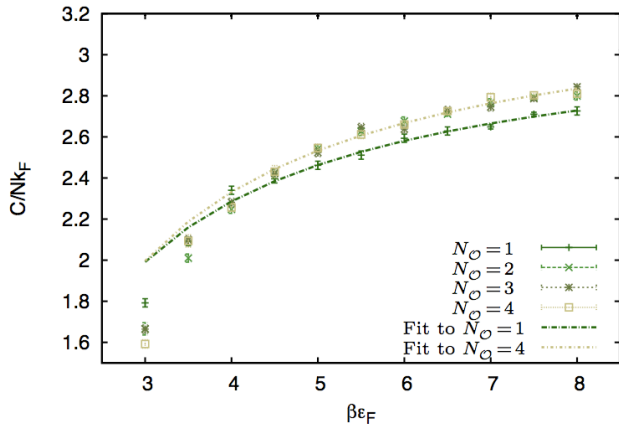


FIG. 5. (Color online) Contact, in units of Nk_F , where $k_F = (3\pi^2 N/V)^{1/3}$ is the Fermi momentum, as a function of the extent of the time direction $\beta\epsilon_F = \tau N_T \epsilon_F$, for 80 particles and levels of improvement $N_O = 1 - 4$. Also shown are fits to the $N_O = 1$ and $N_O = 4$ datasets using the first two terms in the asymptotic form of the previous section (see text for details).

energy. Our extrapolations to the ground state yield $\xi \equiv E/E_{FG} = 0.467(2)$ for the unimproved case, and $\xi = 0.402(1), 0.399(2), 0.399(2)$ for $N_O = 2, 3, 4$, respectively. This change, of roughly 15%, is in line with our expectations based on the large-scale calculations of Ref. [11]. While these results are still roughly 5% greater than those of Ref. [11], which found $\xi \approx 0.38$, it is remarkable that this can be achieved with a 10^3 lattice. The remaining effects must be a combination of finite volume and finite imaginary-time step τ effects.

A similar situation is observed for the contact. Using the extrapolation formula of the previous section at leading plus next-to leading order, we obtain $C/(Nk_F) = 3.17(3)$ in the unimproved case, and $C/(Nk_F) = 3.31(4), 3.34(4)$ and $3.30(4)$ for $N_O = 2, 3, 4$, respectively. (We have discarded three data points at the lowest values of $\beta\epsilon_F$ for the purpose of capturing the asymptotic behavior at large β ; the fits are stable against further removal of points at low $\beta\epsilon_F$). While the latter extrapolations clearly overlap when taking the uncertainty into account, they do not overlap with the unimproved case, which is clearly consistent with what we see in Fig. 5 at large β . The remaining systematic errors, likely due to volume effects for the most part, appear to be only as large as 3%, if we consider the most recent estimates of the contact in the ground state (≈ 3.39 , see Ref. [24]). As in the case of the energy, it is remarkable that such a small volume as 10^3 already yields a result that is quite close to the best current estimate.

In conclusion, we have presented a methodology based on the work of Refs. [4, 5], whereby one can generate not only improved transfer matrices but also improved operators, which account for finite-range effects in a systematic fashion. The improvement program can be carried out in

a Galilean invariant or in a Galilean non-invariant way. We have chosen the latter because it provides a better approach to the unitary limit. As shown in Appendix B, the difference in the eigenvalues of the invariant and non-invariant transfer matrices is very small, such that the effect can be safely considered to be negligible. This is likely due to the fact that the lattice already breaks Galilean invariance. With the chosen improvements in place, we see a large change for the energy but a rather small change for the contact. Indeed, once finite-range effects are under control, the dominant contribution to systematic uncertainties is expected to be given by finite-volume effects. If so, the latter appear to be relatively small both for the energy (roughly 5%) as well as for the contact (roughly 3%).

While we have focused on the unitary limit, the tuning procedure for the transfer matrix and the operators can easily be applied to systems away from unitarity as well as away from the zero effective-range limit. In combination with hybrid Monte Carlo (HMC) techniques, which have recently made it possible to access larger volumes than ever before (as large as 20^3), we expect the method presented here to provide a powerful strategy to tackle the non-relativistic many-fermion problem. This applies in particular to finite-temperature calculations where lowering the ultraviolet cutoff (while keeping effective-range effects under control) reduces the size of the basis, speeding up the computations considerably.

In this regard, it should also be pointed out that improving the transfer matrix affects the performance of the HMC algorithm only marginally. Indeed, the scaling with system size (particle number, spacetime volume) remains unchanged when increasing N_O . Only the prefactor in the scaling law increases somewhat (by about 20 – 25%) due to the need for extra Fourier transforms when applying the operator $A(p)$. Aside from this, the force in the molecular dynamics (MD) part of the HMC algorithm becomes somewhat larger when $A(p)$ is improved, such that somewhat smaller MD time steps (not to be confused with τ) are needed. In short, the performance of the HMC algorithm is largely unaffected by the use of improved transfer matrices.

Finally, we would like to stress that the operator proposed here for the calculation of the contact (based on the derivative of the two-body energy, in turn computed using Eq. (41)) constitutes a novel way to calculate C in MC calculations. This method should be contrasted with others based on extracting the derivative of the equation of state via finite differences, using the momentum distribution, or using the pair distribution function. Each of these will, in general, behave differently in terms of their systematic effects.

ACKNOWLEDGMENTS

Thanks are in order to J. Carlson, W. Detmold, T. Lähde, D. Lee, Y. Nishida, E. Passemar, and S. Tan for

discussions and/or critical comments on the manuscript. I am especially indebted to E. R. Anderson, for numerous discussions that led to this work, and to A. N. Nicholson for clarifications on the work of Ref. [4]. I would also like to thank the Institute for Nuclear Theory in Seattle, WA, as well as the ‘‘Quarks, Hadrons and Nuclei’’ group at the University of Maryland, where some of the early work and discussions took place. This work was supported in part by U.S. Department of Energy, Office of Nuclear Physics under contract DE-FC02-07ER41457 (UNEDF SciDAC).

Appendix A: Evaluation of $\mathcal{S}(\eta)$.

There are many ways to evaluate the function $\mathcal{S}(\eta)$ efficiently. The one that I have found easiest to implement and understand is essentially the one communicated to me by Shina Tan, which I reproduce here, with some minor modifications that I have found useful.

The first step is to enhance the convergence of the sum by introducing an exponential factor and separating the singularity in the tail (see Ref. [22]):

$$\sum_{|\mathbf{n}| < \Lambda} \frac{1}{n^2 - \eta^2} = \sum_{|\mathbf{n}| < \Lambda} \frac{1 - e^{-x(n^2 - \eta^2)}}{n^2 - \eta^2} + \sum_{|\mathbf{n}| < \Lambda} \frac{e^{-x(n^2 - \eta^2)}}{n^2 - \eta^2}, \quad (\text{A1})$$

where $n = |\mathbf{n}|$, the sums are over all triplets of integers \mathbf{n} , and x is a small positive parameter. The second sum has no convergence problems, in fact it converges very quickly, so we shall put it aside by defining

$$\tilde{\mathcal{S}}(\eta, x) \equiv \lim_{\Lambda \rightarrow \infty} \sum_{|\mathbf{n}| < \Lambda} \frac{e^{-x(n^2 - \eta^2)}}{n^2 - \eta^2}. \quad (\text{A2})$$

The first sum, on the other hand, converges just as slowly as the original one (once we subtract the $4\pi\Lambda$ term). Let us then analyze this first sum. For $0 < x \ll 1$, we may approximate it very accurately in terms of an integral:

$$\sum_{|\mathbf{n}| < \Lambda} \frac{1 - e^{-x(n^2 - \eta^2)}}{n^2 - \eta^2} \simeq 4\pi \int_0^\Lambda dn \frac{n^2 (1 - e^{-x(n^2 - \eta^2)})}{n^2 - \eta^2}, \quad (\text{A3})$$

where we have used the spherical symmetry of the integrand. Writing

$$\frac{n^2}{n^2 - \eta^2} = 1 + \frac{\eta^2}{n^2 - \eta^2}, \quad (\text{A4})$$

we separate the integrals into two terms. First,

$$4\pi \int_0^\Lambda dn (1 - e^{-x(n^2 - \eta^2)}) = 4\pi\Lambda - 4\pi e^{x\eta^2} \int_0^\Lambda dn e^{-xn^2}, \quad (\text{A5})$$

TABLE IV. First 30 roots of $\mathcal{S}(\eta)$, and $d\mathcal{S}/d\eta^2$ evaluated at those roots.

k	η_k^2	$d\mathcal{S}/d\eta_k^2$
1	-0.0959007	123.82387
2	0.4728943	39.75514
3	1.4415913	82.36519
4	2.6270076	106.24712
5	3.5366199	84.23133
6	4.2517060	161.88763
7	5.5377008	212.49220
8	7.1962632	62.95336
9	8.2879537	231.79580
10	9.5345314	247.82611
11	10.5505341	233.82976
12	11.7014957	185.61411
13	12.3102392	183.65019
14	13.3831152	316.68684
15	15.3537375	82.86757
16	16.1218253	506.59914
17	17.5325415	371.40245
18	18.6053932	308.00372
19	19.5186394	255.97969
20	20.4033187	329.98905
21	21.6944179	394.81924
22	23.0194727	94.98929
23	24.3306210	342.25749
24	25.3016129	526.27127
25	26.6803600	514.90705
26	27.8780019	150.20773
27	29.6156511	548.38017
28	31.3536974	114.02114
29	32.1958982	443.21169
30	33.4483351	452.78989

where the $4\pi\Lambda$ cancels with the $-4\pi\Lambda$ term in Eq. (3), and the integral in the second term is equal to $1/2\sqrt{\pi/x}$ in the limit $\Lambda \rightarrow \infty$. Second, we have

$$\mathcal{I} \equiv 4\pi \int_0^\Lambda dn \frac{\eta^2 (1 - e^{-x(n^2 - \eta^2)})}{n^2 - \eta^2}. \quad (\text{A6})$$

To treat this term we write

$$1 - e^{-x(n^2 - \eta^2)} = x(n^2 - \eta^2) \int_0^1 dy e^{-xy(n^2 - \eta^2)} \quad (\text{A7})$$

and exchange the order of integration of y and n , to obtain

$$\mathcal{I} = 4\pi x \eta^2 \int_0^1 dy e^{xy\eta^2} \int_0^\Lambda dn e^{-xyn^2}, \quad (\text{A8})$$

all of which can be easily evaluated in the limit $\Lambda \rightarrow \infty$, where the full result can be written as

$$\mathcal{S}(\eta) = \tilde{\mathcal{S}}(\eta, x) - \frac{2\pi^{3/2}}{\sqrt{x}} \left(e^{x\eta^2} - 2x\eta^2 \int_0^1 dt e^{x\eta^2 t^2} \right), \quad (\text{A9})$$

which is to be evaluated for $0 < x \ll 1$.

With the above expressions at hand, it is straightforward to find the first derivative of \mathcal{S} with respect to η^2 :

$$\frac{d\mathcal{S}}{d\eta^2} = \frac{d\tilde{\mathcal{S}}}{d\eta^2} - 2\pi^{3/2}\sqrt{x} \left(e^{x\eta^2} - 2 \int_0^1 dt e^{x\eta^2 t^2} (1 + x\eta^2 t^2) \right), \quad (\text{A10})$$

where

$$\frac{d\tilde{\mathcal{S}}}{d\eta^2} = x\tilde{\mathcal{S}}(\eta) + \lim_{\Lambda \rightarrow \infty} \sum_{|\mathbf{n}| < \Lambda} \frac{e^{-x(n^2 - \eta^2)}}{(n^2 - \eta^2)^2}. \quad (\text{A11})$$

Table IV shows the first 30 roots of $\mathcal{S}(\eta)$, along with the corresponding values of the derivative $d\mathcal{S}/d\eta^2$.

Appendix B: Galilean invariance vs. non-invariance.

One cannot fail to notice that not only is the transfer matrix of Eq. (16) not symmetric, an issue we managed to deal with above, it is also not fully Galilean invariant. Indeed, while translation and rotation invariance are preserved (in their discrete forms set by the lattice), Galilean-boost symmetry is broken. This is because we have assumed that A was promoted to an operator that acts on everything that appears to its right.

On the other hand, if we assume that A acts on the auxiliary field only, as in Ref. [4], one arrives directly at a local, Galilean-invariant lattice theory. Indeed, in that case Eq. (16) changes form in a very simple manner, namely the function $A(\mathbf{p}_\uparrow)$ is replaced by $A(\mathbf{p}_\uparrow - \mathbf{q}_\uparrow)$, and similarly for the other spin. The function A has then a clear physical significance as the momentum transfer in a two-body collision.

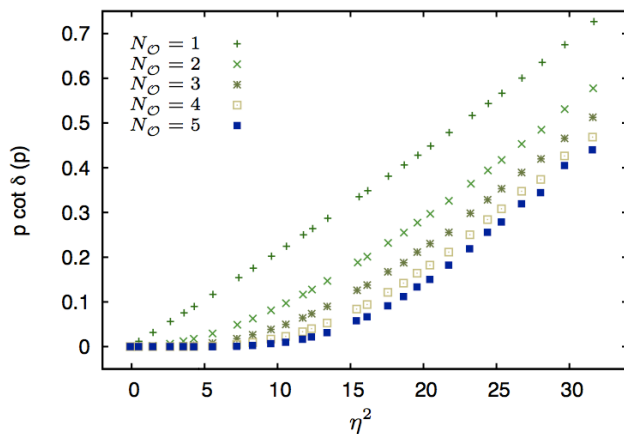


FIG. 6. (Color online) Plot of $p \cot \delta(p)$, in lattice units, as a function of $\eta^2 = E_2/p_0^2$ (where $p_0 \equiv 2\pi/L$), for $N_x = 20$, $\tau = 0.05$, and levels of improvement $N_C = 1-5$, for a Galilean invariant definition of the transfer matrix.

Apart from the obvious desirability of Galilean invariance, these observations seem to indicate that one should

choose this form over the non-invariant version. However, when comparing the approach to the unitary point based on improvements, as shown in Figs. 1 and 6, it is clear that the non-invariant version is much superior to its invariant counterpart. Furthermore, comparing with the results of Ref. [4], it seems clear that one would need much larger lattices in the Galilean invariant version to make Fig. 6 look like Fig. 1, which we have checked with our codes. (Note that Fig. 2 in Ref. [4] presents the same kind of plot but corresponding to a much larger lattice size, namely $N_x = 32$.)

The reason for this difference is likely due to the fact that (discrete) Galilean invariance is only respected in an infinite lattice volume. Indeed, in any *finite* lattice the center-of-mass and relative motions are actually *not* separable. Boosting to frames of different total momentum will, in general, result in Hilbert spaces of vastly different dimensions for the subspace of relative motion. In particular, the zero total momentum Hilbert space, used to tune our two-body interaction, has by far the highest dimension. Based on this assessment, we decided to focus on the non-invariant form in this work.

Should one choose to implement the Galilean invariant form instead, as in Ref. [4], there are two technical details that should not be overlooked. First, in Eq. (16) the function $A(\mathbf{p}_\uparrow)$ becomes $A(\mathbf{p}_\uparrow - \mathbf{q}_\uparrow)$ and therefore needs to be evaluated outside the single-particle momentum lattice where we originally defined it (c.f. Eq. (13)). The extension to the larger domain should be done respecting the periodicity of the momentum lattice.

Second, if such a periodicity is to be reconciled with the continuum form of the non-interacting dispersion relation, which we assumed to be $E = p^2/2m$, we should impose a spherically symmetric cutoff Λ in momentum space. This last condition should have little impact on the results in practice, as long as the systems under consideration are somewhat dilute. From the point of view of computational performance, however, such a restriction on phase space results in important gains, particularly at finite temperature, where all the elements in the basis are evolved in imaginary time.

Regardless of the form of the action, it is possible to evaluate the degree to which Galilean invariance is broken by taking the improved transfer matrix and computing its eigenvalues in a moving frame. As long as Galilean invariance is respected, inserting the eigenvalues into the Rummukainen-Gottlieb formula [25] should yield the same scattering phase shift as Lüscher's formula. This will of course include breaking effects coming from both the action *and* the lattice itself.

Here, we limit ourselves to comparing the eigenvalues obtained from the invariant and non-invariant formulations, in various frames. In Fig. 7 we show a plot of the relative eigenvalue difference $|\Delta E_n/E_n|$ between the Galilean invariant and non-invariant improved transfer matrices, evaluated in various moving frames (i.e. non-zero center-of-mass momentum). As can be appreciated in that plot, the difference between the invariant and non-

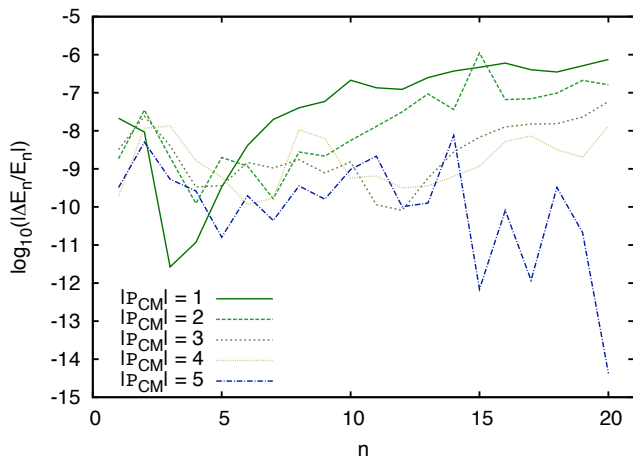


FIG. 7. (Color online) Logarithmic plot of the relative eigenvalue difference $|\Delta E_n/E_n|$ between the Galilean invariant and non-invariant improved transfer matrices, as a function of the eigenvalue index n , in various moving frames. The quantity \mathbf{P}_{CM} denotes the center-of-mass momentum, in units of $2\pi/L$. This data set corresponds to $N_x = 18$, $\tau = 0.05$, $N_{\mathcal{O}} = 3$.

invariant improvements is extremely small, which shows that one can use the non-invariant version of the improvement program without introducing a noticeable systematic effect.

-
- [1] I. Montvay, G. Münster, *Quantum fields on the lattice* (Cambridge University Press, New York, NY, 1994); H. Rothe, *Lattice Gauge Theories*, 3rd ed. (World Scientific, Singapore, 2005). T. DeGrand and C. DeTar, *Lattice Methods for Quantum Chromodynamics* (World Scientific, Singapore, 2006).
- [2] P. Lepage, Lectures given at the VIII Jorge Andre Swieca Summer School (Brazil, 1997); arXiv:nucl-th/9706029. G. P. Lepage, in *Proceedings of TASI'89: From Actions to Answers*, T. DeGrand and D. Toussaint (eds.) (World Scientific, 1989); arXiv:hep-ph/0506330v1.
- [3] K. Symanzik, Nucl. Phys. B **226**, 187 (1983); *ibid.* **226**, 205 (1983).
- [4] M. G. Endres, D. B. Kaplan, J.-W. Lee, A. N. Nicholson, Phys. Rev. A **84**, 043644 (2011).
- [5] M. G. Endres, D. B. Kaplan, J.-W. Lee, A. N. Nicholson, PoS (Lattice 2010) 182. J.-W. Lee, M. G. Endres, D. B. Kaplan, A. N. Nicholson, PoS (Lattice2010) 197. A. N. Nicholson, M. G. Endres, D. B. Kaplan, J.-W. Lee, PoS (Lattice2010) 206.
- [6] *Ultracold Fermi Gases*, Proceedings of the International School of Physics “Enrico Fermi”, Course CLXIV, Varenna, June 20 – 30, 2006, M. Inguscio, W. Ketterle, C. Salomon (Eds.) (IOS Press, Amsterdam, 2008).
- [7] M. Lüscher, Commun. Math. Phys. **105**, 153 (1986).
- [8] R. L. Stratonovich, Sov. Phys. Dokl. **2** (1958) 416; J. Hubbard, Phys. Rev. Lett. **3** (1959) 77.
- [9] J.W. Negele and H. Orland, *Quantum Many-Particle Systems* (Addison-Wesley, Redwood City, CA, 1988).
- [10] A. Privitera, M. Capone, C. Castellani, Phys. Rev. B **81**, 014523 (2010); A. Privitera, M. Capone, Phys. Rev. A **85**, 013640 (2012).
- [11] J. Carlson, S. Gandolfi, K. E. Schmidt, S. Zhang, Phys. Rev. A **84**, 061602(R) (2011).
- [12] S. Bour, X. Li, D. Lee, Ulf-G. Meissner, and L. Mitas, Phys. Rev. A **83**, 063619 (2011).
- [13] J. Braun, S. Diehl, and M. M. Scherer, Phys. Rev. A **84**, 063616 (2011).
- [14] A. Bazabov, D. Toussaint, C. Bernard, J. Laiho, C. DeTar, L. Levkova, M. B. Oktay, U. M. Heller, J. E. Hetrick, P. B. Mackenzie, R. Sugar, R. S. Van de Water, Rev. Mod. Phys. **82**, 1349 (2010).
- [15] A. Bulgac, J. E. Drut, P. Magierski, Phys. Rev. Lett. **99** (2007) 120401; Phys. Rev. Lett. **96** (2006) 090404; Phys. Rev. A **78** (2008) 023625; P. Magierski, G. Wlazłowski, A. Bulgac, J. E. Drut, Phys. Rev. Lett. **103** (2009) 210403.
- [16] J. E. Drut, T. A. Lähde, T. Ten, Phys. Rev. Lett. **106**, 205302 (2011).
- [17] J. E. Drut, T. A. Lähde, G. Wlazłowski, P. Magierski, Phys. Rev. A **85**, 051601(R) (2012).
- [18] R. Blankenbecler, D. J. Scalapino, R. L. Sugar, Phys. Rev. D **24**, 2278 (1981).
- [19] D. Lee, Phys. Rev. C **78**, 024001 (2008); Prog. Part. Nucl. Phys. **63**, 117 (2009).
- [20] S. Tan, Ann. Phys. **323**, 2952 (2008); *ibid.* **323**, 2971 (2008); *ibid.* **323**, 2987 (2008).
- [21] E. Braaten, *Universal Relations for Fermions with Large Scattering Length*, in *The BCS-BEC crossover and the Unitary Fermi Gas* W. Zwerger (ed.) (Springer, Berlin, 2011); arXiv:1008.2922.
- [22] S. Tan, Phys. Rev. A **78**, 013636 (2008).
- [23] J. Zinn-Justin, *Quantum Field Theory and Critical Phenomena* (Oxford University Press, New York, 2002).
- [24] S. Gandolfi, K. E. Schmidt, J. Carlson, Phys. Rev. A **83**, 041601(R) (2011).
- [25] K. Rummukainen, S. Gottlieb, Nucl. Phys. B **450**, 397 (1995); C.h. Kim, C.T. Sachrajda, S. R. Sharpe, Nucl. Phys. B **727**, 218 (2005).